High-power femtosecond mid-IR sources for s-SNOM applications

2014 J. Opt. 16 094003

(http://iopscience.iop.org/2040-8986/16/9/094003)

IOP Publishing Journal of Optics
J. Opt. **16** (2014) 094003 (7pp) doi:10.1088/2040-8978/16/9/094003

INVITED ARTICLE

High-power femtosecond mid-IR sources for s-SNOM applications

R Hegenbarth[1], A Steinmann[1], S Mastel[2,3], S Amarie[3], A J Huber[3], R Hillenbrand[2,4], S Y Sarkisov[5] and H Giessen[1]

[1] 4th Physics Institute and Research Center SCoPE, University of Stuttgart, Pfaffenwaldring 57, D-70550 Stuttgart, Germany
[2] CIC nanoGUNE Consolider, E-20018 Donostia—San Sebastián, Spain
[3] Neaspec GmbH, D-82152 Planegg, Germany
[4] IKERBASQUE, Basque Foundation for Science, E-48011 Bilbao, Spain
[5] Functional Electronics Laboratory, National Research Tomsk State University, 634050 Tomsk, Russia

E-mail: robin.hegenbarth@physik.uni-stuttgart.de

Received 31 March 2014, revised 16 May 2014
Accepted for publication 2 June 2014
Published 3 September 2014

Abstract

We demonstrate two high-power femtosecond mid-infrared (mid-IR) sources that can be combined with a scattering-type scanning near-field optical microscope (s-SNOM). The first one is based on difference frequency generation (DFG) between the two signal wavelengths of a high-power dual-signal-wavelength periodically poled lithium niobate (PPLN) optical parametric oscillator (OPO) and covers the spectral range from 10.5 μm to 16.5 μm. The second one is an $AgGaSe_2$ OPO pumped by the PPLN OPO. With this mid-IR OPO we obtained up to 113 mW average idler power at 4857 nm with more than 40 cm^{-1} FWHM spectral width. We demonstrate mid-IR near-field spectra and near-field images that we obtained by combining the broadband femtosecond mid-IR DFG source with an s-SNOM.

Keywords: nonlinear optics, difference frequency generation, optical parametric oscillators

(Some figures may appear in colour only in the online journal)

1. Introduction

Broadband femtosecond mid-infrared (mid-IR) sources are very promising light sources for scattering-type scanning near-field optical microscopes (s-SNOM), which allow for recording of spatial and spectral information on the nanoscale [1, 2]. Application examples include phonon resonances in semiconductors [3], biominerals [4], polymers [5, 6], quartz [7] or plasmonic resonances in nanoantennas [8]. If more optical power is available, mid-IR near-field microscopy will be more feasible as the scan time will be reduced [2].

Broadband femtosecond mid-IR radiation can be obtained via difference frequency generation (DFG) with two near-infrared sources [9], optical parametric amplifiers [10–12] or with optical parametric oscillators (OPOs) [13–15]. All of these sources rely on the availability of suitable optically nonlinear materials with sufficiently high mid-IR transmittivity and phase-matching capability. DFG sources have been realized by mixing signal and idler from OPOs in crystals such as GaSe [16], $GaS_{0.4}Se_{0.6}$ [17], $LiInSe_2$ [18] or $AgGaSe_2$ [19]. Another approach is based on DFG between fiber-laser systems and Raman-shifted solitons [20–22]. These DFG sources can cover the wavelength range up to 17 μm with typical power levels of a few mW at the longer wavelengths. A few femtosecond OPOs with idler wavelengths longer than 4.5 μm have been published so far. An OPO that employed a mid-IR transmission window of periodically poled lithium niobate (PPLN) to obtain 14.4 mW average idler power at 5.3 μm was demonstrated by [23]. A silver gallium diselenide ($AgGaSe_2$) OPO with an idler

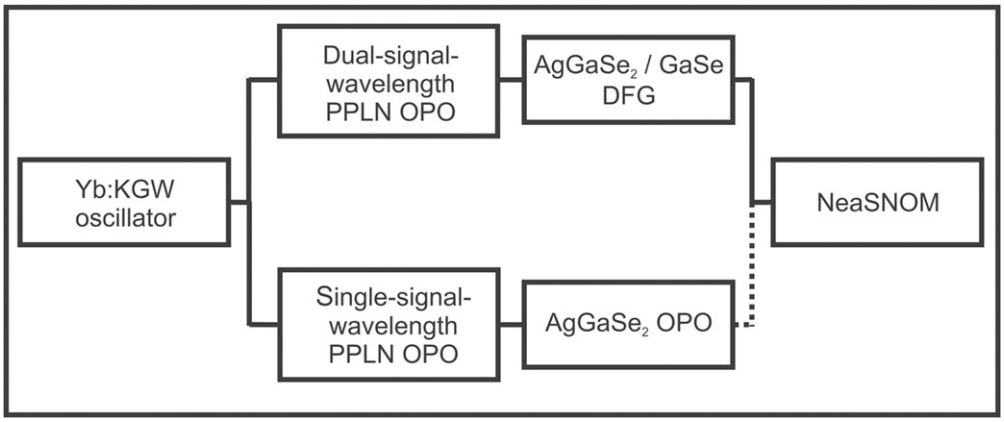

Figure 1. Our experimental setup consisting of two branches for nonlinear frequency conversion into the mid-IR that are pumped by an Yb:KGW oscillator: a PPLN OPO, either operated at two signal wavelengths and followed by a DFG stage comprising an $AgGaSe_2$ or GaSe crystal (see section 2) or operated at a single signal wavelength and followed by a synchronously pumped $AgGaSe_2$ OPO (see section 3). The broadband mid-IR radiation can be employed as a light source for an s-SNOM (see section 5).

tunable between 4 and 8 μm and up to 35 mW pumped by a cesium titanyl arsenate OPO was demonstrated by [24]. An OPO based on an orientation-patterned gallium arsenide crystal pumped by a thulium-doped fiber laser tunable between 2.6 and 6.1 μm with up to 37 mW average idler power was published by [25, 26], while an OPO based on a cadmium silica phosphide crystal with an idler tunable between 5.8 and 6.6 μm with up to 24 mW estimated idler power was demonstrated by [27].

A scheme of our experimental setup is shown in figure 1. We employ an Yb:KGW laser oscillator [28] as pump source of a PPLN OPO followed by two different conversion schemes that can be employed alternatively. In one conversion scheme we operate the OPO at two signal wavelengths [29] followed by DFG. The experimental setup and the results of this DFG setup are thoroughly discussed in [30] and are only briefly summarized in section 2. In the other conversion scheme we employ the signal of the PPLN OPO operated at a single signal wavelength to pump a mid-IR OPO based on an $AgGaSe_2$ crystal, whose idler wavelength can be tuned between 4570 and 5121 nm with up to 113 mW average idler power. This mid-IR OPO is tuned by adjusting cavity length, phase-matching angle or pump wavelength. The properties of its idler output are discussed in section 3. In section 4 we demonstrate the feasibility of combining the broadband femtosecond mid-IR source discussed in section 2 with the NeaSNOM, an s-SNOM provided by Neaspec GmbH.

2. DFG with two signals of a high-power dual-signal-wavelength PPLN OPO

In order to obtain tunable broadband mid-IR radiation beyond 10 μm wavelength, we generate the difference frequency between the two signals of a high-power dual-signal-wavelength PPLN OPO. Since we combined this broadband mid-IR source with an s-SNOM (see section 4), we briefly discuss the experimental setup and the mid-IR power and spectra in this section.

The dual-signal-wavelength OPO is synchronously pumped by an Yb:KGW laser oscillator delivering up to 7.4 W average output power, at 42 MHz repetition rate, 530 fs pulse duration and 1040 nm wavelength. The OPO is based on a 1 mm long magnesium oxide doped PPLN crystal with 31 μm poling period. This OPO is capable of dual-signal-wavelength operation, since its total intracavity group delay dispersion (GDD) equals zero at the center of the tuning range (1740 nm), resulting in two different signal wavelengths with identical group delay that oscillate simultaneously. The two signal wavelengths can be tuned between 1563 and 1621 nm and between 1795 and 1859 nm, respectively. Up to 1.45 W average signal output power can be achieved with 34:66 power splitting ratio with this configuration.

The difference frequency between these two signals can either be generated in a 3 mm long $AgGaSe_2$ crystal cut for 49° phase-matching angle and type-II phase-matching, in a 3.1 mm long anti-reflection coated GaSe crystal, or in a 1 mm long z-cut GaSe crystal. In the case of $AgGaSe_2$ and the anti-reflection coated GaSe crystal the polarization of the shorter wavelength beam is rotated by 90° to obtain efficient type-II phase-matching. In the case of the 1 mm long GaSe crystal identical polarizations of both OPO wavelengths are employed. The latter setup is more compact, but conversion is less efficient. In this case the polarization is rotated by 45°, so that the horizontal projection of the polarization of the shorter wavelength beam and the vertical projection of the polarization of the longer wavelength beam are optimized.

The mid-IR power as a function of wavelength of this DFG system is shown in figure 2(a). Up to 4.3 mW average power has been obtained at 13.2 μm (758 cm^{-1}) by using a 3 mm long $AgGaSe_2$ crystal, while up to 1.2 mW has been obtained at 11.92 μm (839 cm^{-1}) by using a 1 mm long GaSe crystal. Up to 1.3 mW has been obtained at 14.1 μm (709 cm^{-1}) by using a 3.1 mm long anti-reflection coated GaSe crystal. Its front side was coated with an SiO_2 layer with 260 nm thickness generated by thermal evaporation. This coating causes between 1% and 8% reflectivity for the signal of the near-IR OPO, depending on wavelength. The rear side

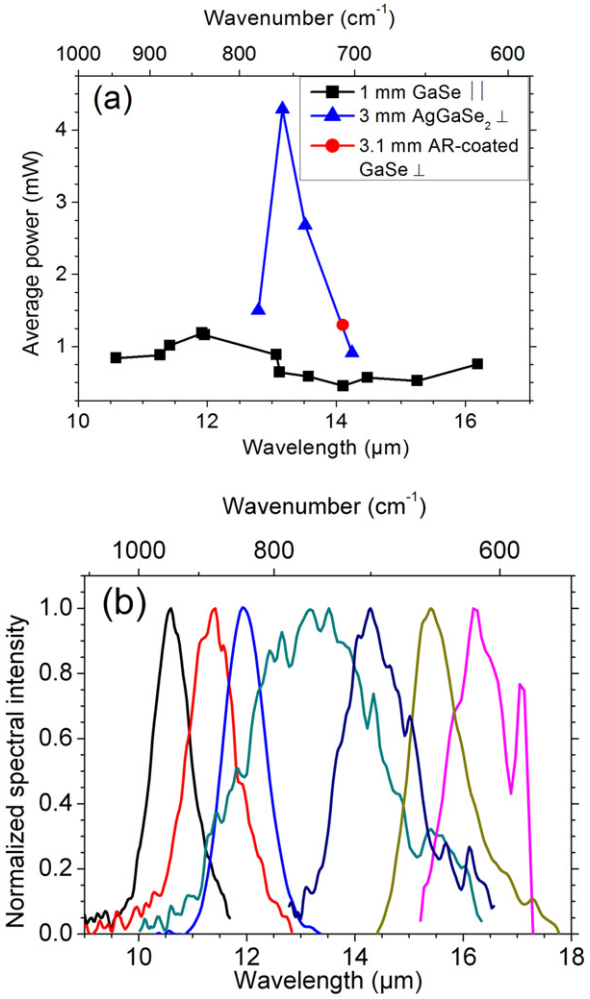

Figure 2. (a) Average mid-IR power as a function of wavelength and wavenumber obtained with the DFG setup by employing either a 3 mm long $AgGaSe_2$ crystal and perpendicular polarizations of the two OPO signals (blue triangles), a 1 mm long GaSe crystal and parallel polarizations of the two OPO signals (black squares), or a 3.1 mm long anti-reflection coated GaSe crystal (red circle). (b) Mid-IR spectra obtained with 1 mm long GaSe.

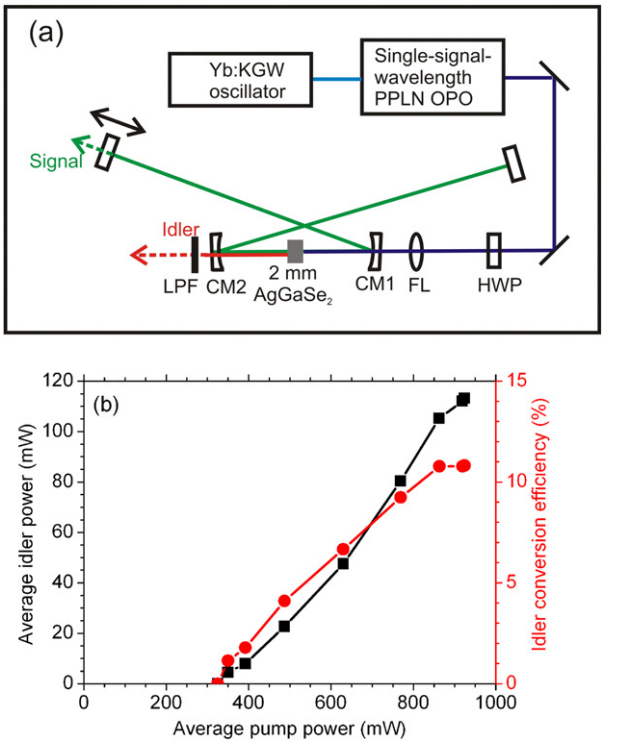

Figure 3. (a) Experimental setup of the mid-IR OPO consisting of an Yb:KGW oscillator that synchronously pumps a single-signal-wavelength PPLN OPO that in turn synchronously pumps an $AgGaSe_2$ mid-IR OPO. (b) Average idler power (black squares) and the corresponding idler power conversion efficiency (red circles) as a function of average pump power.

of this crystal features an anti-reflective oxidation layer [31] created by extended exposure of the crystal at 400 K temperature in an H_2O atmosphere. Its reflectivity is below 10% in the mid-IR spectral region accessed in this experiment, which is better than the Fresnel reflections.

The corresponding mid-IR spectra generated by using 1 mm long GaSe are shown in figure 2(b). The spectra are broadband with more than 50 cm^{-1} FWHM spectral width. The system is tunable between 10.5 and 16.5 μm (952–606 cm^{-1}).

3. Femtosecond $AgGaSe_2$ mid-IR OPO pumped by a high-power PPLN OPO

The experimental setup of the $AgGaSe_2$ mid-IR OPO is shown in figure 3(a). A 7.4 W output Yb:KGW oscillator with 42 MHz repetition rate is employed as pump source to synchronously pump the PPLN OPO that comprises a 1 mm long MgO-doped PPLN crystal with 30 μm poling period. At this configuration it emits up to 1.25 W average signal output power with approximately 450 fs pulse and a single signal wavelength tunable between 1538 and 1607 nm. This signal beam is employed to pump the $AgGaSe_2$ OPO and is referred to as a pump beam in the remainder of this publication. A half-wave plate is employed to adjust pump polarization for type-I phase-matching, where the pump beam is polarized extraordinarily and the signal and idler beams are polarized ordinarily. The pump beam is focused into the $AgGaSe_2$ crystal by means of a focusing lens with 75 mm focal length and a plano-concave dichroic filter (CM1) with 100 mm radius of curvature.

The pump power available in front of the crystal is restricted to below 1 W to avoid crystal damage. The 2 mm long $AgGaSe_2$ crystal is cut for 70° phase-matching angle and 45° azimuthal angle, which is necessary for type-I phase-matching in a crystal of $\bar{4}2$ m, and has a broadband anti-reflection coating for pump, signal and idler wavelengths. The dichroic filters CM1 and CM2 are also employed as cavity mirrors that are highly reflective for the signal. CM2 is additionally employed as an idler output coupling mirror. Thus, it has a CaF_2 substrate with 79% transmittivity at 4857 nm wavelength to provide sufficient idler transmittivity. The cavity consists of four mirrors to provide intracavity signal feedback, one of which is a signal output coupler with

1% signal transmittivity. A long-pass filter (LPF) outside the cavity behind CM2 separates the idler beam from the residual pump beam.

The OPO is tuned by adjusting cavity length, phase-matching angle or pump wavelength. Cavity length adjustment is achieved by adjusting the position of the signal output coupling mirror with a linear translation stage, while adjustment of phase-matching angle is achieved by rotating the $AgGaSe_2$ crystal with a rotation stage. Adjustment of pump wavelength is achieved by changing the cavity length of the PPLN OPO along with an according change of cavity length of the $AgGaSe_2$ OPO.

The average idler power at 4857 nm wavelength (2059 cm^{-1}) and the corresponding idler power conversion efficiency as a function of pump power in front of the crystal are shown in figure 3(b). Up to 113 mW has been obtained, corresponding to 10.8% power conversion efficiency or 38% photon conversion efficiency. The oscillation threshold occurs at 330 mW average pump power. The conversion efficiency saturates at more than 860 mW average pump power or approximately 2.6 times the oscillation threshold. This behavior is consistent with the theory for OPOs with uniform plane waves published by [32].

Idler spectra for different cavity lengths at 1566 nm pump wavelength and perpendicular pump beam incidence on the crystal, corresponding to 70° phase-matching angle, are shown in figure 4(a). A larger relative change of cavity length means a longer cavity. At shorter cavity lengths the idler wavelength decreases when increasing the cavity length, which corresponds to increasing signal wavelength. At longer cavity lengths the idler wavelength increases with increasing cavity length. This behavior can be explained by zero intracavity signal GDD at the wavelength at which the direction of the shift changes. With this method the idler wavelength can be tuned between 4797 and 5121 nm (2085–1953 cm^{-1}). The FWHM idler spectral width ranges between 38 and 95 cm^{-1}. This corresponds to a Fourier limit of 150–390 fs assuming Gaussian pulses. The spectra are broader at intermediate cavity lengths.

The average idler power as a function of relative change of cavity length is shown in figure 4(b). The OPO is operated over 56 μm relative change of cavity length. Up to 111 mW idler power has been achieved at 4820 nm (2075 cm^{-1}) and the FWHM power tuning range is approximately 140 nm or 60 cm^{-1}. This corresponds to 30 μm relative change of cavity length.

Idler spectra at different phase-matching angles and 1566 nm pump wavelength are shown in figure 4(c). The OPO is operational over 1.7° change of phase-matching angle, which corresponds to 4.4° change of angle of incidence. At smaller phase-matching angles (69.7–70°) the idler wavelength decreases at increasing phase-matching angles. At larger phase-matching angles (70–71.4°) the idler wavelength increases at increasing phase-matching angles. With this method the idler wavelength can be tuned between 4814 and 5026 nm (2077–1990 cm^{-1}). The FWHM spectral width ranges between 49 and 123 cm^{-1}. This corresponds to a Fourier limit of 120–300 fs assuming Gaussian pulses. The spectra are broader at shorter phase-matching angles.

The average idler power as a function of phase-matching angle is shown in figure 4(d). Up to 113 mW has been achieved at 4857 nm (2059 cm^{-1}) and the FWHM idler phase-matching bandwidth is approximately 1.4°. This corresponds to 170 nm or 80 cm^{-1} FWHM power tuning range.

Idler spectra at different pump wavelengths and 70° phase-matching angle are shown in figure 4(e). At each pump wavelength the cavity length was adjusted to obtain optimum idler power. The OPO is operational at pump wavelengths between 1540 and 1577 nm at that configuration. The idler wavelength decreases at increasing pump wavelength. This tuning behavior can be explained by the wavelength dependence of the refractive index of $AgGaSe_2$.

With this method the idler wavelength can be tuned between 4570 and 5005 nm (2189–1998 cm^{-1}). The FWHM idler spectral width ranges between 54 and 84 cm^{-1}. This corresponds to a Fourier limit of 175–270 fs assuming Gaussian pulses. The average idler output power as a function of idler wavelength and wavenumber is shown in figure 4(d). Up to 113 mW has been achieved at 4843 nm (2065 cm^{-1}). The FWHM power tuning range is as large as 330 nm (140 cm^{-1}).

4. Combination of a broadband femtosecond mid-IR source with an s-SNOM

We employed the broadband femtosecond mid-IR source described in section 2 as a source of radiation for a scattering-type SNOM [1]. In addition to obtaining near-field images, this device is capable of recording near-field spectra with a nano-FTIR spectrometer [4] by the light backscattered from the oscillating tip of the s-SNOM with a Michelson interferometer, in which the sample is located in one of the interferometer arms [33].

In the following paragraphs experimental results obtained with this combination will be discussed. These results have been obtained by demodulating the detector signal of the 280 kHz tip oscillation frequency, which reduces background scattering [1].

A near-field interferogram and the corresponding near-field spectrum of gold at a center frequency around 795 cm^{-1} (12.58 μm) are shown in figures 5(a) and (b), respectively. Due to a lack of absorption features the shape of this spectrum is equivalent to the spectrum of the DFG source. These results show that the signal-to-noise ratio of the interferogram and of the spectrum are good enough to combine the broadband mid-IR source with the nano-FTIR spectrometer.

The topography and the near-field image of a silicon-doped gallium nitride (GaN) nanowire are shown in figures 5(c) and (d), respectively. The pixels on these two images are rectangular with 100 nm edge length. The near-field signal was obtained by illuminating the tip with the radiation, the corresponding spectrum is shown in figure 5(b). The light backscattered from the tip was recorded without the interferometer. The changes of the near-field signal along the

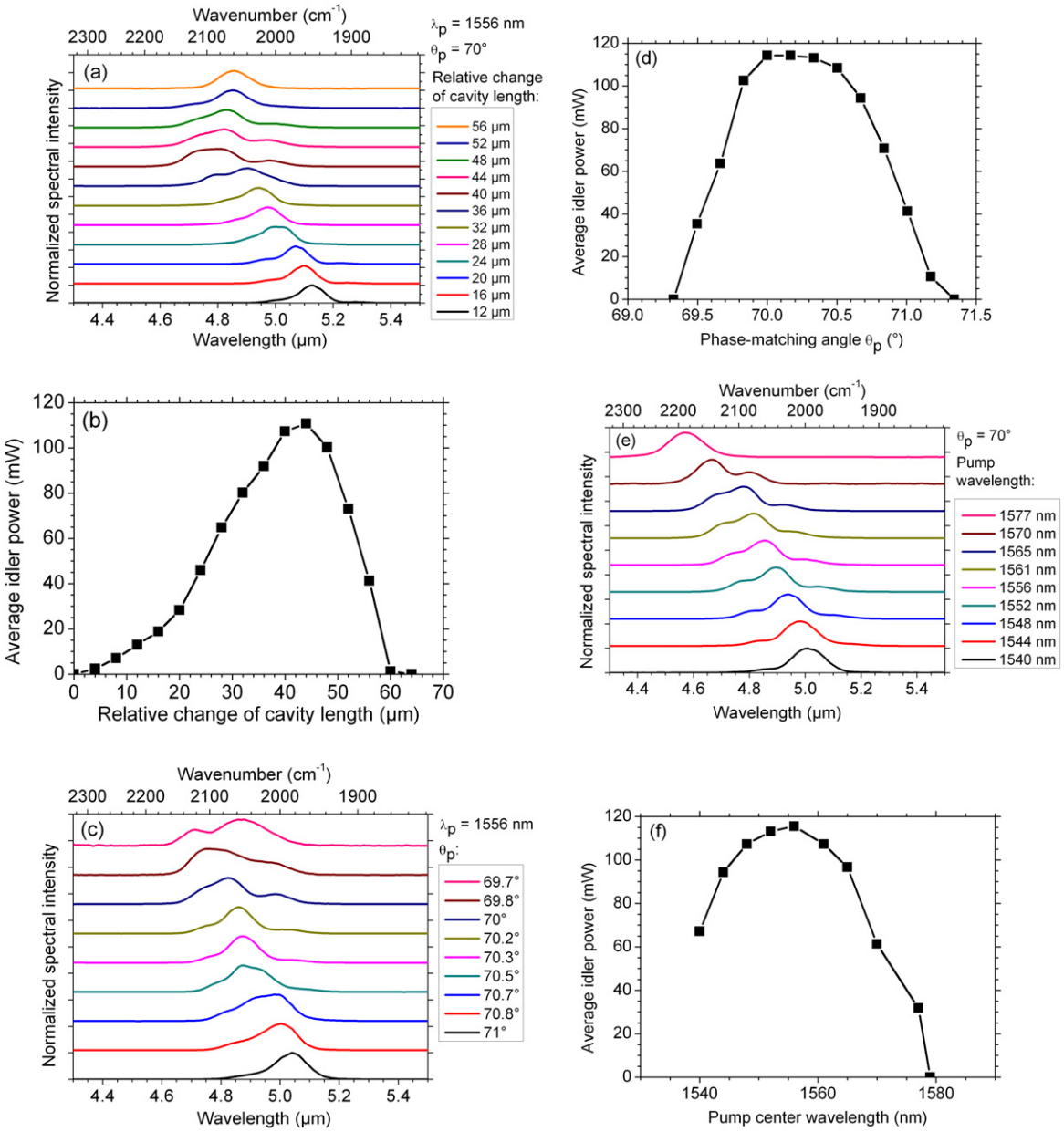

Figure 4. Idler spectra (a) and the corresponding average idler power as a function of relative change of cavity length (b) when tuning the cavity length at 1566 nm pump wavelength and 70° phase-matching angle. Idler spectra (c) and the corresponding average idler power (d) as a function of phase-matching angle when tuning the phase-matching angle at 1566 nm pump wavelength. Idler spectra (e) and the corresponding average idler power (f) as a function of pump wavelength when tuning the pump wavelength at 70° phase-matching angle.

wire indicate a variation of the dielectric properties, which might be due to crystal defects or variations in local doping [34]. Nano-FTIR spectroscopic mapping of nanowires is expected to provide further insights in the future.

The topography and the near-field image of a silicon carbide (SiC)/gold interface, recorded analogous to figures 5(c) and (d), but at a center frequency of about 690 cm^{-1} (14.5 μm), are shown in figures 5(e) and (f), respectively. The pixels on the latter two images are rectangular with 50 nm edge length. Gold appears bright due to its higher mid-IR reflectivity compared to SiC in this frequency range.

These two examples show that a combination of this broadband mid-IR source based on DFG between the two OPO signal wavelengths with a near-field microscope is feasible.

5. Conclusions

We demonstrated two high-power femtosecond mid-IR sources. One of them is based on DFG between the two signal wavelengths of a high-power femtosecond OPO that can be operated at two different signal wavelengths due to zero intracavity GDD at the center of the tuning range. By

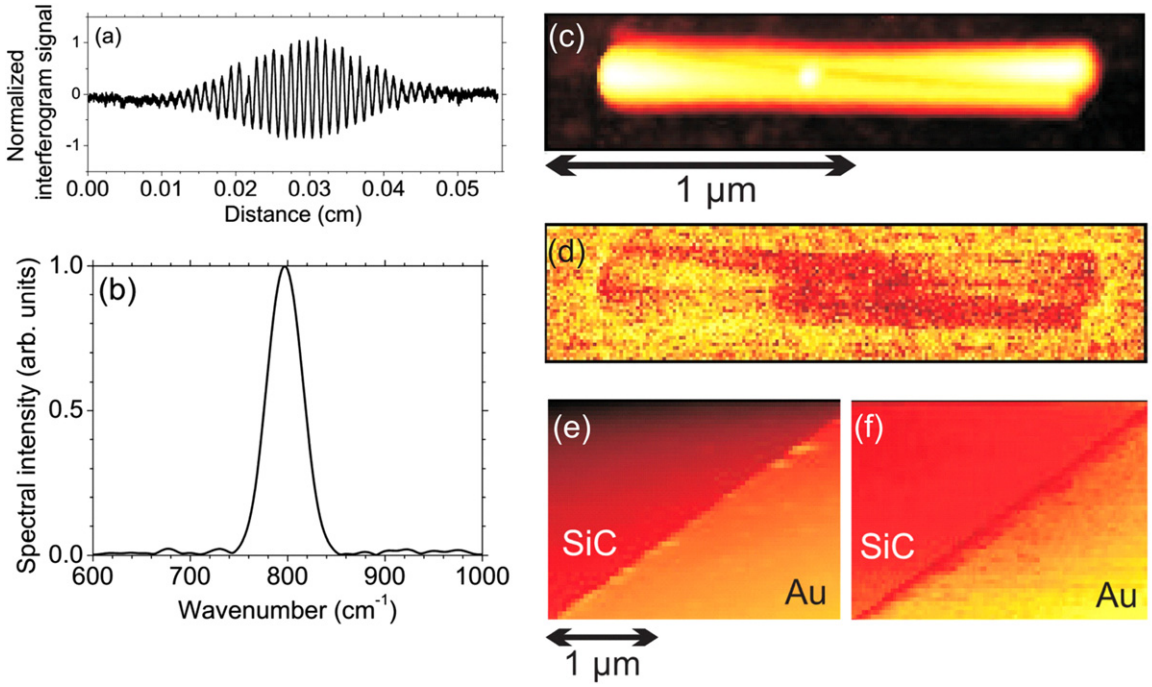

Figure 5. A near-field interferogram (a) and the corresponding near-field spectrum (b) of gold at 795 cm^{-1} (12.58 μm). The topography (c) and simultaneously recorded near-field signal (d) of a silicon-doped gallium nitride nanowire (d) at a center frequency of about 795 cm^{-1}. The topography (e) and the corresponding near-field signal (f) of a silicon carbide (SiC)/gold (Au) interface recorded at a center frequency of about 690 cm^{-1} (14.5 μm).

employing a 3 mm long $AgGaSe_2$ crystal for DFG, up to 4.3 mW has been obtained at 13.2 μm. This system is tunable between 10.5 and 16.5 μm.

The other one is a mid-IR OPO based on a 2 mm long $AgGaSe_2$ crystal and pumped by the PPLN OPO operated at a single signal wavelength. With this system we have obtained up to 113 mW average idler power at 4857 nm with more than 40 cm^{-1} FWHM spectral width. The idler wavelength of this system is tunable between 4570 and 5121 nm by adjusting cavity length, phase-matching angle or pump wavelength. By choosing crystals cut at other phase-matching angles, the tuning range could be extended in the future.

We demonstrated mid-IR near-field spectra and near-field images that we obtained by combining our broadband femtosecond mid-IR DFG source with an s-SNOM to demonstrate the feasibility of this combination. With this system near-field spectroscopic phonon and strain mapping of various materials as well as fast nano-FTIR spectroscopy become possible.

Acknowledgments

We acknowledge financial support from Baden-Württemberg-Stiftung, Deutsche Forschungsgemeinschaft (DFG FOR730 and SPP1391), Bundesministerium für Bildung und Forschung (13N10146), and from the ERC Advanced Grant COMPLEXPLAS. We thank Martin Eickhoff for providing the GaN nanowire. Sergey Sarkisov acknowledges support by The Ministry of Education and Science of Russia, project N 1206.

References

[1] Keilmann F and Hillenbrand R 2004 Near-field microscopy by elastic light scattering from a tip *Phil. Trans. R. Soc. Lond.* A **362** 787–805
[2] Keilmann F and Amarie S 2012 Mid-infrared frequency comb spanning an octave based on an Er fiber laser and difference-frequency generation *J. Infrared Millim. Terahz Waves* **33** 479–84
[3] Huber A J, Ziegler A, Köck T and Hillenbrand R 2009 Infrared nanoscopy of strained semiconductors *Nat. Nanotechnology* **4** 153–7
[4] Amarie S, Zaslanski P, Kajihara Y, Griesshaber E, Schmahl W W and Keilmann F 2012 Nano-FTIR chemical mapping of minerals in biological materials *Beilstein J. Nanotechnology* **2012** 312–23
[5] Taubner T, Hillenbrand R and Keilmann F 2004 Nanoscale polymer recognition by spectral signature in scattering infrared near-field microscopy *Appl. Phys. Lett.* **85** 5064–6
[6] Hoffmann J M, Hauer B and Taubner T 2012 Antenna-enhanced infrared near-field nanospectroscopy of a polymer *Appl. Phys. Lett.* **101** 193105
[7] Amarie S and Keilmann F 2011 Broadband-infrared assessment of phonon resonance in scattering-type near-field microscopy *Phys. Rev.* B **83** 045404
[8] Mastel S, Grefe S E, Cross G B, Taber A, Dhuey S, Cabrini S, Schuck P J and Abate Y 2012 Real-space mapping of nanoplasmonic hotspots via optical antenna-gap loading *Appl. Phys. Lett.* **101** 131102
[9] Erny C, Moutzouris K, Biegert J, Kühlke D, Adler F, Leitenstorfer F and Keller U 2007 Mid-infrared difference-frequency generation of ultrashort pulses tunable between 3.2 and 4.8 μm from a compact fiber source *Opt. Lett.* **32** 1138–40
[10] Cerullo G and De Silvestri S 2003 Ultrafast optical parametric amplifiers *Rev. Sci. Instrum.* **74** 1–18

[11] Krauth J, Steinmann A, Hegenbarth R, Conforti M and Giessen H 2013 Broadly tunable femtosecond near- and mid-IR source by direct pumping of an optical parametric amplifier with a 41.7 MHz Yb:KGW oscillator *Opt. Express* **21** 11516–22
[12] Marangoni M, Osellane R, Ramponi R, Cerullo G, Steinmann A and Morgner U 2007 Near-infrared optical parametric amplifier at 1 MHz directly pumped by a femtosecond oscillator *Opt. Lett.* **32** 1489–91
[13] Adler F, Cossel K C, Thorpe M J, Hartl I, Fermann M E and Ye J 2009 Phase-stabilized, 1.5 W frequency comb at 2.8–4.8 μm *Opt. Lett.* **34** 1330–2
[14] Hebling J, Mayer E J, Kuhl J and Szipöcs J 1995 Chirped-mirror dispersion-compensated femtosecond optical parametric oscillator *Opt. Lett.* **20** 919–21
[15] Südmeyer T, Innerhofer E, Brunner F, Paschotta R, Usami T, Ito H, Kurimura S, Kitamura K, Hanna D C and Keller U 2004 High-power femtosecond fiber-feedback optical parametric oscillator based on periodically poled stoichiometric $LiTaO_3$ *Opt. Lett.* **29** 1111–3
[16] Ehret S and Schneider H 1998 Generation of subpicosecond infrared pulses tunable between 5.2 μm and 18 μm at a repetition rate of 76 MHz *Appl. Phys.* B **66** 27–30
[17] Beutler M, Rimke I, Büttner E, Panyutin V and Petrov V 2013 80 MHz difference-frequency generation of femtosecond pulses in the mid-infrared using $GaS_{0.4}Se_{0.6}$ *Laser Phys. Lett.* **10** 075406
[18] Beutler M, Rimke I, Büttner E, Petrov V and Isaenko L 2013 Femtosecond mid-IR difference-frequency generation in $LiInSe_2$ *Opt. Mater. Express* **3** 1834–8
[19] Beutler M, Rimke I, Büttner E, Badikov V, Badikov D and Petrov V 2014 Efficient femtosecond 50 MHz repetition rate mid-IR source up to 17 μm by difference-frequency generation in $AgGaSe_2$ *Proc. SPIE* **8964** 8964–11
[20] Ruehl A, Gambetta A, Hartl I, Fermann M E, Eikema K S E and Marangoni M 2012 Widely-tunable mid-infrared frequency comb source based on difference frequency generation *Opt. Lett.* **37** 2232–4
[21] Gambetta A, Coluccelli N, Cassinerio M, Gatti D, Laporta P, Galzerano G and Marangoni M 2013 Milliwatt-level frequency combs in the 8–14 μm range via difference frequency generation from an Er:fiber oscillator *Opt. Lett.* **38** 1155–7
[22] Phillips C R *et al* 2012 Widely tunable midinfrared difference frequency generation in orientation-patterned GaAs pumped with a femtosecond Tm-fiber system *Opt. Lett.* **37** 2928–30
[23] Loza-Alvarez P, Brown C T A, Reid D T and Sibbett W 1999 High-repetition-rate ultrashort-pulse optical parametric oscillator continuously tunable from 2.8 to 6.8 μm *Opt. Lett.* **24** 1523–5
[24] Marzenell S, Beigang R and Wallenstein R 1999 Synchronously pumped femtosecond optical parametric oscillator based on $AgGaSe_2$ tunable from 2 μm to 8 μm *Appl. Phys.* B **69** 423–8
[25] Leindecker N, Marandi A, Byer R L, Vodopyanov K L, Jiang J, Hartl I, Fermann M and Schunemann P G 2013 Octave-spanning ultrafast OPO with 2.6–6.1 μm instantaneous bandwidth pumped by femtosecond Tm-fiber laser *Opt. Express* **20** 7046–53
[26] Lee K F, Jiang J, Mohr C, Bethge J, Fermann M E, Leindecker N, Vodopyanov K L, Schunemann P G and Hartl I 2013 Carrier envelope offset frequency of a doubly resonant, nondegenerate, mid-infrared GaAs optical parametric oscillator *Opt. Lett.* **38** 1191–3
[27] Zhang Z, Reid D T, Chaitanya Kumar S, Ebrahim-Zadeh M, Schunemann P G, Zawilski K T and Howle C R 2013 *Opt. Lett.* **38** 5110–3
[28] Steinmann A, Metzger B, Hegenbarth R and Giessen H 2011 Compact 7.4 W femtosecond oscillator for white-light generation and nonlinear microscopy *Conf. on Lasers and Electro-Optics, OSA Technical Digest (CD)* (Washington, DC: Optical Society of America) paper CThAA5
[29] Hegenbarth R, Steinmann A, Tóth G, Hebling J and Giessen H 2011 Two-color femtosecond optical parametric oscillator with 1.7 W output pumped by a 7.4 W Yb:KGW laser *J. Opt. Soc. Am.* B **28** 1344–52
[30] Hegenbarth R, Steinmann A, Sarkisov S and Giessen H 2012 Milliwatt-level mid-infrared (10.5 μm–16.5 μm) difference frequency generation with a femtosecond dual-signal-wavelength optical parametric oscillator *Opt. Lett.* **37** 3513–5
[31] Drapak S I, Gavrylyuk S V, Kovalyuk Z D and Lytvyn O S 2008 Native oxide emerging of the cleavage surface of gallium selenide due to prolonged storage *Semiconductors* **42** 414–21
[32] Bjorkholm J E 1971 Some effects of spatially nonuniform pumping in pulsed optical parametric oscillators *IEEE J. Quantum Electron.* **7** 109–18
[33] Huth F, Govyadinov A, Amarie S, Nuansing W, Keilmann F and Hillenbrand R 2012 Nano-FTIR absorption spectroscopy of molecular fingerprints at 20 nm spatial resolution *Nano Lett.* **12** 3973–8
[34] Stiegler J M, Huber A J, Diedenhofen S L, Gomez Rivas J, Algra R E, Bakkers E P A M and Hillenbrand R 2010 Nanoscale free-carrier profiling of individual semiconductor nanowires by infrared near-field nanoscopy *Nano Lett.* **10** 1387–92